

See discussions, stats, and author profiles for this publication at: <https://www.researchgate.net/publication/266029329>

# Molecular Simulation of the Concentration-Dependent Interaction of Hydrophobic Drugs with Model Cellular Membranes

ARTICLE in THE JOURNAL OF PHYSICAL CHEMISTRY B · SEPTEMBER 2014

Impact Factor: 3.3 · DOI: 10.1021/jp5047613 · Source: PubMed

---

CITATION

1

READS

22

## 2 AUTHORS:



[Myungsim Kang](#)

City University of New York - College of Staten ...

26 PUBLICATIONS 370 CITATIONS

[SEE PROFILE](#)



[Sharon M. Loverde](#)

CUNY Graduate Center

41 PUBLICATIONS 278 CITATIONS

[SEE PROFILE](#)

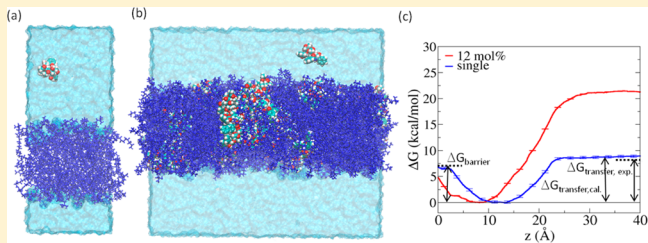
# Molecular Simulation of the Concentration-Dependent Interaction of Hydrophobic Drugs with Model Cellular Membranes

Myungshim Kang and Sharon M. Loverde\*

Department of Chemistry, College of Staten Island, The City University of New York, 2800 Victory Boulevard, Staten Island, New York 10314, United States

 Supporting Information

**ABSTRACT:** We report here the interactions between a hydrophobic drug and a model cellular membrane at the molecular level using all-atom molecular dynamics simulations of paclitaxel, a hydrophobic cancer drug. The calculated free energy of a single drug across the bilayer interface displays a minimum in the outer hydrophobic zone of the membrane. The transfer free energy shows excellent agreement with reported experimental data. In two sets of long-time simulations of high concentrations of drug in the membrane (12 and 11 mol %), the drugs display substantial clustering and rotation with significant directional preference in their diffusion. The main taxane ring partitions in the outer hydrophobic zone, while the three phenyl rings prefer to be closer to the hydrophobic core of the membrane. The clustering of the drug molecules, order parameters of the lipid tails, and water penetration suggest that the fluidity and permeability of the membrane are affected by the concentration of drugs that it contains. Furthermore, at the high-concentration limit, the free energy minimum shifts closer to the hydrophobic core and the central barrier to cross the membrane decreases. Moreover, the transfer free energy change substantially increases, suggesting that increasing concentration facilitates drug partitioning into the membrane.



## INTRODUCTION

Cell membranes are often the main and often final barriers in drug delivery. However, it is not well-known how most hydrophobic drugs (such as paclitaxel) penetrate through cell membranes. For example, solutes are known to pass through the membrane with a passive or a more active cooperative mechanism<sup>1</sup> such as pore formation. In this paper we characterize the molecular level interactions of paclitaxel, an anticancer drug, with a model lipid membrane.

A phospholipid membrane is an inhomogeneous environment consisting of a low dielectric material in a high dielectric medium, water. Overton observed a correlation between the membrane permeability coefficient of a solute and its oil–water partition coefficient.<sup>2,3</sup> Considering the transverse heterogeneity of the lipid membrane, the solubility–diffusion model relates the membrane permeability  $P$  to the depth  $z$ -dependent parameters of the diffusion constant  $D(z)$  and partition coefficient  $K(z)$  of a solute along with the membrane thickness  $h$ .<sup>4,5</sup> Furthermore, the membrane permeability has been shown to be susceptible to the solute concentration in the membrane.<sup>2,6–9</sup>

Paclitaxel is the first identified microtubule-stabilizing agent.<sup>10</sup> It binds to the microtubule to promote polymerization of tubulin and shifts the assembly equilibrium, inducing mitotic arrest and consequent apoptosis.<sup>11–13</sup> Clinically, it is used to treat solid tumors such as breast, ovarian, lung, pancreatic, gastroesophageal, head, and neck cancer. This hydrophobic cancer drug aggregates in both hydrophobic and hydrophilic

environments.<sup>14,15</sup> Additionally, it has been suggested that it induces the formation of stable pores in the membrane at high concentration.<sup>16</sup> The poor water solubility of paclitaxel limits its clinical application, as in most hydrophobic drugs. Currently, it is dissolved in a surfactant or formulated as an albumin-bound suspension. While these formulations are somewhat effective in increasing the injectable dose, they involve serious side effects, and there are concerns in gaining an accurate quantitative control and optimization of their pharmacokinetic profile. Significant efforts have gone into nanocarrier formulations for the delivery of hydrophobic drugs.<sup>17–23</sup> For example, liposomal drug delivery has been widely investigated, where a drug is encapsulated within liposomes or drug carriers to improve the pharmacokinetics and biodistribution profile of the drug.<sup>24</sup> By manipulating specific factors, such as the size, shape, and surface decoration of these carriers, their targeting selectivity, loading and unloading efficiency, and ability to enter the cell have been extensively tested.<sup>25–30</sup> Modeling the transport of hydrophobic drugs through the cell membrane will help us understand the fundamental interactions between the hydrophobic drug and the biomembrane, leading to the design of optimized drug delivery systems.<sup>31,32</sup>

The packing and interactions between paclitaxel molecules are both solvent and concentration dependent.<sup>14,15</sup> Further-

Received: May 14, 2014

Revised: September 19, 2014

Published: September 22, 2014

more, the perturbation of the drug to the membrane structure is also suggested to be concentration dependent. Experimentally, it has been shown that at drug concentrations of less than 2 mol % in a dipalmitoylphosphatidylcholine (DPPC) membrane, the liquid crystalline to gel transition temperature broadens due to the paclitaxel location in the outer hydrophobic domain zone of the membrane.<sup>33</sup> However, at higher concentrations, the transition temperature begins to drop due to the drug partitioning deeper into the hydrophobic region of the membrane. At even higher concentrations (>10 mol %), it is observed that the drug aggregates and phase separates.<sup>34</sup> These observations indicate the concentration-dependent nature of paclitaxel partitioning in membranes. Additionally, a concentration-dependent nature was observed for curcumin partitioning<sup>35</sup> as well as ibuprofen partitioning.<sup>36</sup> This suggests that the behavior might be universal and described by a simple two-phase model:<sup>35</sup> two separate populations of drug, one population at the membrane interface and one population deeper in the core of the membrane. Increasing the concentration of drug perturbs the membrane structure and environment. Therefore, the interaction of additional drugs with the perturbed membrane environment will be altered.

Herein, we investigate the interactions between paclitaxel and a model cellular membrane composed of 1-palmitoyl-2-oleoyl-sn-glycero-3-phosphocholine (POPC) at the molecular level using long-time all-atom molecular dynamics simulations (~350 ns). POPC is chosen since it is a model lipid found in the cell membrane and is commonly used for biophysical measurements. Furthermore, we investigate the drug transfer free energy from the solvent (water) to the membrane utilizing adaptive biasing force (ABF) methodology<sup>37,38</sup> in two different cases. In the first case, as schematically shown in Figures 1a and 2a, we investigate the free energy profile of

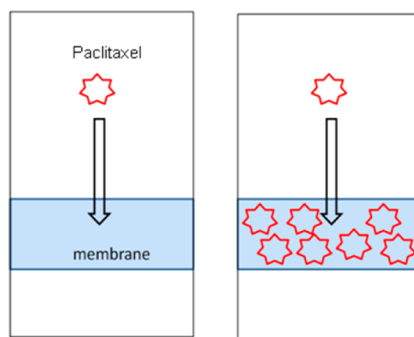


**Figure 1.** Schematic of paclitaxel insertion into the membrane: (a, left) insertion into a pure POPC lipid membrane, (b, right) insertion into a POPC membrane with 12 mol % paclitaxel.

paclitaxel with a pure POPC lipid membrane. In the second case, as schematically shown in Figures 1b and 2b, we investigate the free energy profile of paclitaxel with a POPC membrane containing 12 mol % paclitaxel. The profile of free energy across the membrane exhibits a shift in the free energy minimum closer to the hydrophobic core of the membrane with increasing concentration of drug. Moreover, the central barrier to cross the leaflets decreases. Finally, the transfer free energy of drug from water to the membrane substantially increases at increased drug concentrations. Modeling the transport of hydrophobic drugs into the cell through computational investigations will provide molecular-level insight into the

drug distribution process and help the design of delivery vehicles that facilitate drug delivery.

## METHODS

**Simulation Systems.** The two pure POPC bilayer membrane systems consisted of 59 POPC and 3433 water molecules in one system and 640 POPC and 35160 water molecules in the other one. The single paclitaxel molecule and POPC membrane system consisted of 1 paclitaxel molecule, 59 POPC molecules, and 5268 water molecules. Two high-concentration paclitaxel systems were built: the random model and the lattice model. The random model was constructed by randomly inserting paclitaxel molecules into the POPC membrane and then removing any overlapping POPC molecules, which was followed by solvation of the membrane. Both the orientation and the position of the drug were random. The resulting structure contained 60 paclitaxel, 420 POPC, and 41152 water molecules, ending up with a 12 mol % drug system (see Figure 3a,e). The lattice model followed the same procedure as that of the random model, except that paclitaxel molecules were inserted at lattice points of each layer of the POPC membrane with a single orientation (see also Figure 3c,g). After removal of the overlapped POPC molecules and solvation, the lattice model contained 60 paclitaxel, 483 POPC, and 41242 water molecules, resulting in 11 mol % drug.

**Molecular Dynamics Simulation Parameters and Conditions.** The CHARMM36 force field<sup>39,40</sup> was used for POPC,<sup>41</sup> and the CHARMM TIP3P model (also known as the TIP3P model)<sup>42,43</sup> was used for water. For paclitaxel, the force field parametrized by David Sept<sup>44</sup> was used. MD simulations were carried out using NAMD2.<sup>45</sup> All systems used the NPT ensemble and Langevin dynamics<sup>46</sup> at a temperature of 310 K with a damping coefficient  $\gamma = 1 \text{ ps}^{-1}$  at a pressure of 1 atm using an anisotropic Langevin piston method<sup>46,47</sup> with a piston period of 200 fs and a damping time scale of 50 fs. The SHAKE algorithm was used to hold covalent bonds involving hydrogen rigid, allowing a 2 fs time step. The particle mesh Ewald (PME) algorithm<sup>48</sup> was employed to take full electrostatic interactions into account, with full periodic boundary conditions. The cutoff for van der Waals interactions was 12 Å with a smooth switching function at 10 Å used to truncate the van der Waals potential energy at the cutoff distance. Coordinates were saved every 2 ps for the trajectory analysis. The two pure POPC bilayer membrane systems and the single paclitaxel molecule in POPC were run for 101, 110, and 100 ns, respectively. The random and lattice models were simulated for 346 and 352 ns, respectively.

**Free Energy Calculations.** The free energy of paclitaxel was calculated using the ABF method.<sup>38,49</sup> In ABF, a running average in the appropriate bin gives an estimation of the mean force  $\langle F_\xi | \xi^* \rangle = -dA(\xi^*)/d\xi$  along the order parameter  $\xi$ . Then, to oppose the mean force, an external force,  $-\langle F_\xi | \xi^* \rangle \nabla \xi$ , is applied, causing the system to undergo a random walk without barriers along the order parameter. This procedure leads to uniform sampling of  $\xi$ . The ABF calculations here were based on two drug concentrations: single paclitaxel in POPC and the 12 mol % random model system after 100 and 320 ns of normal MD simulations, respectively. The initial configuration of each window for the ABF method was selected from the trajectories obtained from the steered molecular dynamics (SMD) simulations (see the Supporting Information for details). ABF was performed for 40 ns for each 2.5 Å window. The calculated potential of mean force (PMF) converges within

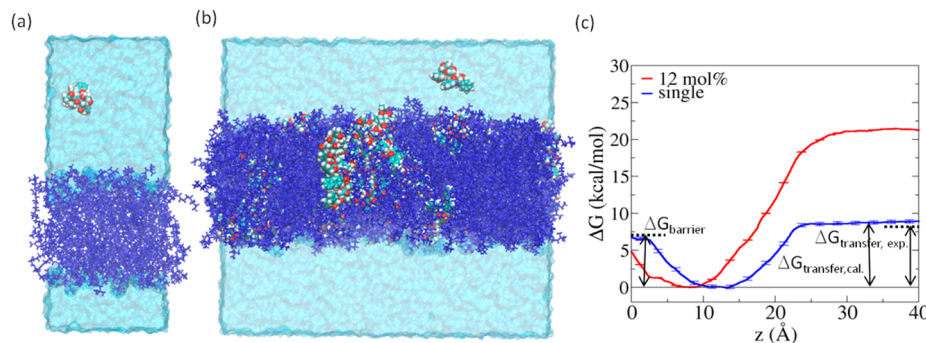


**Figure 2.** Concentration-dependent profile of the free energy of paclitaxel across the bilayer interface: (a) a single paclitaxel molecule (CPK colored spacing-filling model) with a pure POPC membrane (dark blue) and water (light blue), (b) 12 mol % paclitaxel–POPC membrane system in a random position, (c)  $\Delta G$  vs  $z$  of a single paclitaxel molecule (black) and 12 mol % paclitaxel (red). The standard deviation in the central bin of each window with a width of 0.1 Å is shown.

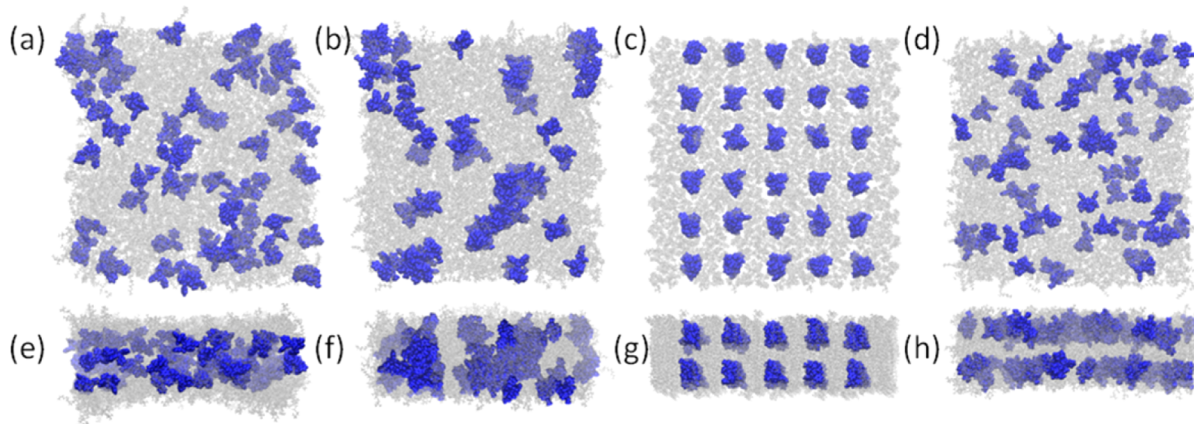


**Figure 3.** Snapshots of two sets of high-concentration drug systems: initial (a, e) and final (b, f) views of the random model of 12 mol % drug, initial (c, g) and final (d, h) views of the lattice model of 11 mol % drug. The top row displays the top views and the bottom row the side views. Paclitaxel and POPC molecules are displayed in blue and gray, respectively. Water molecules are not shown for clarity.

40 ns (see Figure S1 in the Supporting Information for the PMF, sample counts, and gradients as a function of the simulation time per window).

## RESULTS AND DISCUSSION

To begin with, we calculate the interaction free energy of the drug across the POPC bilayer interface utilizing the ABF methodology in two different environments as shown in Figure 2: a pure POPC bilayer (Figure 2a) and POPC with over 12 mol % paclitaxel (Figure 2b). The two free energy curves are shown in Figure 2c. The free energy profile of a single paclitaxel molecule in the POPC bilayer (Figure 2c) displays a minimum in the outer hydrophobic zone of the bilayer, 13.4 Å from the center of mass of the bilayer. The free energy change ( $\Delta G_{\text{transfer}}$ ) from water to the bilayer is  $8.9 \pm 0.23$  kcal/mol, in excellent agreement with 7.9 kcal/mol measured by Wenk et al.<sup>50</sup> Furthermore, the profile exhibits a barrier ( $\Delta G_{\text{barrier}}$ ) in the hydrophobic core of  $6.8 \pm 0.23$  kcal/mol to translocate from one leaflet to the other leaflet. The profile for paclitaxel insertion into the membrane substantially shifts (Figure 2c) when additional concentration of drug is included in the membrane.

At a high randomly distributed paclitaxel concentration of 12 mol % in the membrane,  $\Delta G_{\text{transfer}}$  significantly increases to  $21.2 \pm 0.05$  kcal/mol, indicating increased partitioning of the drug in the membrane over water. Most notably, the central barrier ( $\Delta G_{\text{barrier}}$ ) in the hydrophobic core decreases to  $4.4 \pm 0.05$

kcal/mol, making it easier for the drug to cross the hydrophobic core at these high concentrations. Additionally, the minimum shifts closer to the inner hydrophobic core, at 8.4 Å. A “permeability predictor”,  $P_{\Delta G}$ , has been proposed to predict and quantify the permeability using  $\Delta G_{\text{max}}$  and  $\Delta G_{\text{min}}$ , the maximum and minimum values, respectively, of the transfer free energy profile, along with the Boltzmann constant  $k_B$  and the temperature  $T$ :<sup>51</sup>  $P_{\Delta G} = k_B T / (\Delta G_{\text{max}} - \Delta G_{\text{min}})$ . At 12 mol % the difference between  $\Delta G_{\text{max}}$  and  $\Delta G_{\text{min}}$  actually increases to 21.2 kcal/mol, compared to 8.9 kcal/mol in the single-drug system, resulting in a decrease of  $P_{\Delta G}$  from 0.07 to 0.04 to predict that the permeability of the drug decreases. Given the partition coefficient  $K(z) = e^{-\Delta G(z)/RT}$ , the permeability can be estimated using the average diffusion coefficient in the  $z$  direction ( $D_z$ ) in the solubility–diffusion model, which also indicates a decrease of the permeability at 12 mol %. The two predictions are consistent with each other since the permeability predictor was derived from the solubility–diffusion model.<sup>4</sup>

One assumption for this model is that both sides of the membrane are water. However, in the cell, the intracellular environment is substantially more crowded than the outside of the membrane. A variety of biomolecules, such as transmembrane proteins and cholesterol, exist within the cell membrane.<sup>52–55</sup> This crowding effect inside and within the cell membrane may break the symmetry of the free energy profile and change the membrane properties, shifting  $\Delta G_{\text{transfer}}$ .

Another assumption within the scope of this paper is that cooperative drug effects—drug aggregation within the water prior to insertion—play a negligible role. However, recent computational studies have shown that cooperative effects<sup>56,57</sup> can play an essential role in membrane insertion. Interestingly, the limiting step in the whole membrane-crossing process of the drug is the core crossing ( $\Delta G_{\text{barrier}}$ ) in the middle in the single-drug system, with the final step ( $\Delta G_{\text{transfer}}$ ) from the membrane head region to the bulk water of the other side at high concentration. Altogether, these changes in the free energy profile suggest that the distribution and the transportability of the drug in the membrane are affected by the concentration, making drug insertion into the hydrophobic zone of the membrane significantly more favorable at high concentrations.

To determine which favorable interactions are driving the shift in interaction free energy between paclitaxel and the other system components (membrane, water, and drug), we decompose the intermolecular interactions of the selected paclitaxel molecule with each system component as shown in Figure S2 (Supporting Information). The interaction energy between the selected paclitaxel molecule and the rest of the paclitaxel molecules is shown in Figure 4a. We find that both

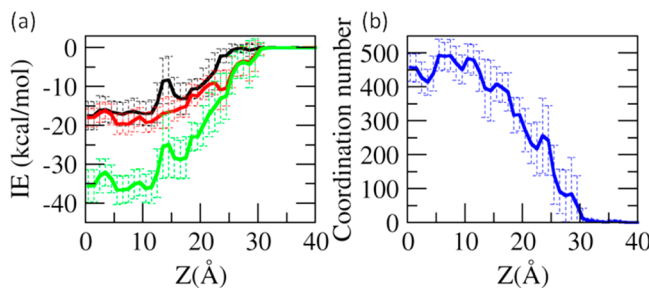


**Figure 4.** (a) Interaction energy between the inserted paclitaxel molecule and the rest of the drug molecules as a function of the distance  $Z$  from the center of mass of the membrane. ES, denoted by the solid black line, is the electrostatic interaction. VDW, denoted by the solid red line, is the van der Waals interaction.  $E_{\text{total}}$ , denoted by the solid green line, is the total interaction energy. (b) Coordination number between the inserted paclitaxel and the rest of the drug molecules as a function of the distance  $Z$  from the center of mass of the membrane.

the electrostatic and van der Waals interactions between the drugs act in stabilizing the incoming paclitaxel in the membrane with a net change in the interaction energy of 35 kcal/mol at these high concentrations of paclitaxel. The paclitaxel–paclitaxel interaction becomes increasingly favorable as the paclitaxel approaches the center of mass of the membrane. We note that this is higher than the reported enthalpic contribution for paclitaxel binding at low concentrations as reported by Wenk et al.<sup>50</sup> Furthermore, as the drug approaches the hydrophobic core of the membrane, the interaction of the selected paclitaxel molecule with POPC increases, mainly due to van der Waals interactions (Figure S2). Meanwhile, the drug–water interaction energy decreases. The total electrostatic interactions are non-negligible in the hydrophobic core due to the lower dielectric permittivity of the medium. This is correlated to an increase in the coordination number of the paclitaxel with the rest of the drug molecules (Figure 4b). We define the coordination number as  $c_{AB} = \sum_{i \in A} \sum_{j \in B} [1 - (r_{ij}/d_0)^6]/[1 - (r_{ij}/d_0)^{12}]$ , where A and B are the species of atoms,  $r_{ij}$  are the interatomic distances, and  $d_0$  is the cutoff distance of

4 Å.<sup>58</sup> At the high-concentration limit, as intuitively expected, the paclitaxel molecule gains increasing contacts with neighboring drug molecules, while losing contacts with the POPC molecules in turn. The sum of the interactions of the selected paclitaxel molecule with the system components (membrane, water, and drug) does not completely account for the free energy difference from the water phase to the membrane phase, suggesting an entropic contribution to the free energy. The order parameter of the POPC tails is discussed later as an indirect indicator of the entropic contribution.

The configuration of neighboring paclitaxel in the membrane may shift the free energy profile. For this reason, we characterize paclitaxel aggregation over time in two separate simulations: 12 mol % paclitaxel that is randomly inserted into the membrane and paclitaxel at approximately the same mole fraction (11 mol %) that starts from a lattice configuration. Both the random and lattice models show aggregation over a time scale of 346 ns as shown in Figure 3. The random model starts with randomly inserted drugs (Figure 3a,e) and results in transbilayer clusters (Figure 3b,f). The drug molecules form small clusters with 3–6 drug molecules as early as 1 ns, and then the small clusters merge to build up larger aggregates with up to 15 molecules at 10 ns. The growth of the small clusters is extremely fast (within the first 10 ns of simulation), but then the growth of the clusters becomes more gradual (Figure S3, Supporting Information). The lattice model begins with drugs initially inserted at lattice points with a single orientation (Figure 3c,g). The drugs show comparably less initial aggregation than the random model, but still continue to aggregate after a simulation time of 352 ns (Figures 3d,h and S3).

We hypothesize that the random model is closer to the equilibrium limit and that if the simulation time is long enough, the lattice model will approach a configuration similar to that of the random model. While the clusters are still growing in the lattice model, the clusters in the random model are larger and their growth becomes gradual, after the quick initial formation. The radial distribution functions  $g(r)$  of an oxygen atom (O13) in the tail side also show an increase in the height of the first peak, indicating increasing contacts between the drug molecules due to aggregation. The radial distribution functions of a single carbon atom (C45) in the main taxane ring show dynamic profiles over the simulation time, suggesting potential rearrangement within the clusters. Additionally, in the lattice model, there is notably less diffusion in the  $z$  direction, given that the starting configuration for the drugs is initially located near the free energy minimum for a single paclitaxel molecule in the membrane as shown in Figure 3g. Since there is a  $\Delta G_{\text{barrier}}$  in the hydrophobic core, the clusters will need to reach a critical size to overcome the barrier and establish transmembrane clusters, akin to the random model. The calculated diffusion coefficients of the drug also support anisotropic directional movements of the drugs. The diffusion coefficient of the drug in the lattice model is almost a factor of 2 larger than that of the random model (Table 1). As the drug clusters grow bigger in the random model, their diffusion slows down. This is as expected according to the Stokes–Einstein relation<sup>59,60</sup>  $D = k_B T / 6\pi\eta r$ , where  $D$  is the diffusion coefficient,  $k_B$  the Boltzmann constant,  $T$  the temperature,  $\eta$  the viscosity, and  $r$  the particle radius. Furthermore, due to the free energy minimum, the lateral diffusion coefficients in the  $xy$  plane ( $D_{xy}$ ) are higher than those along the direction normal to the

**Table 1.** Diffusion Coefficients of Paclitaxel<sup>a</sup>

|                       | random model    | lattice model   |
|-----------------------|-----------------|-----------------|
| D                     | $1.31 \pm 0.02$ | $2.21 \pm 0.59$ |
| $D_z$ <sup>b</sup>    | $0.50 \pm 0.10$ | $0.12 \pm 0.10$ |
|                       | $2.55 \pm 0.95$ |                 |
| $D_{xy}$ <sup>c</sup> | $1.70 \pm 0.09$ | $3.26 \pm 0.86$ |

<sup>a</sup>Units of  $10^{-8} \text{ cm}^2/\text{s}$ . <sup>b</sup>Diffusion coefficients in the  $z$  direction.

<sup>c</sup>Lateral diffusion coefficients in the  $xy$  plane.

membrane interfacial plane ( $D_z$ ) in both the random and lattice models.

This anisotropy in the diffusion can be visualized when the trajectories of a paclitaxel molecule are viewed after removal of the center-of-mass movement of the system, as shown in Figure 5. Parts b, c, e, and f of Figure 5 clearly show more random

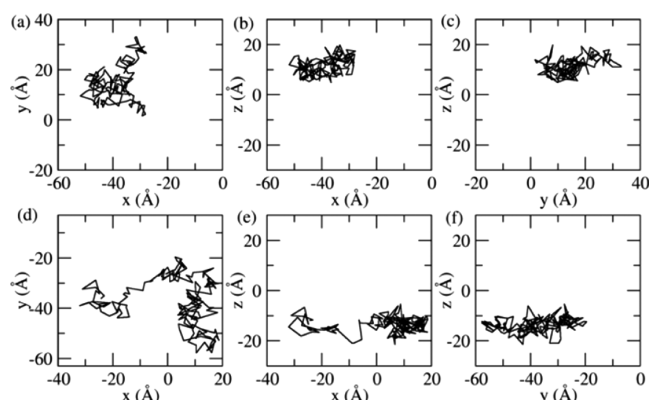


**Figure 5.** Trajectories of a paclitaxel molecule in the membrane in the random (a–c) and lattice (d–f) models on the  $xy$ ,  $xz$ , and  $yz$  planes, respectively.

motion in the  $x$  and  $y$  directions vs the  $z$  direction. This directional difference results from the fact that the  $xy$  plane of the membrane is rather homogeneous, while there is a gradient of the free energy in the  $z$  direction toward a minimum. Another interesting observation is that  $D_z$  exhibits two different

slopes, suggesting double diffusion modes (Figure S5, Supporting Information).

Meyer–Overton's rule for passive transport describes the transmembrane permeability  $P$  as a function of the hydrocarbon/water partition coefficient  $K$ , the diffusion coefficient  $D$ , and the membrane thickness  $h$ :<sup>2,3</sup>  $P = KD/h$ . During the passive transport of a drug/solute across the membrane, the diffusion on the  $z$  axis perpendicular to the membrane plane is important.. The refined version of this model has been proposed to focus on the heterogeneous  $z$  component of the diffusion:<sup>4,5</sup>  $P = 1/\int_{-h/2}^{h/2} d_z/[K(z) D_z(z)]$ . In this case, the higher  $D_z$  of the drug in the random model than the lattice model suggests a higher transmembrane permeability in the random model.

The paclitaxel molecule displays a preferred orientation as well as position along the  $z$  axis, as shown in Figure 6. Each portion of the molecule prefers a different position and orientation in the membrane. The main taxane rings move toward the heads of the lipids, while the three phenyl groups face toward the center of the membrane. This trend is more distinct in the lattice model since the system starts with a single initial orientation of paclitaxel (Figure 6d,e): in the top leaflet, the initial orientation of the drugs remains the same, while the drug in the bottom leaflet displays significant rotation even at 10 ns. The latter ends in  $180^\circ$  rotation after 320 ns of simulation, leading to transmembrane symmetry with the phenyl groups closer to the core of the membrane and the main taxane ring near the headgroup of POPC. This orientational preference of the drug can be explained simply by its hydrophobicity/hydrophilicity that matches the local environments in the membrane. The flexibility of the phenyl rings comes from their carbon chain arms. The random model follows this distribution trend in general so that the phenyl groups are closer to the hydrophobic core and the main taxane ring near the hydrophilic headgroup. However, the distribution of the main taxane ring is broader and does not show any discontinuous gap between the top and bottom leaflets. This corresponds well with the PMF profile, where the free energy minimum shifts toward the core and the central barrier  $\Delta G_{\text{barrier}}$  decreases.

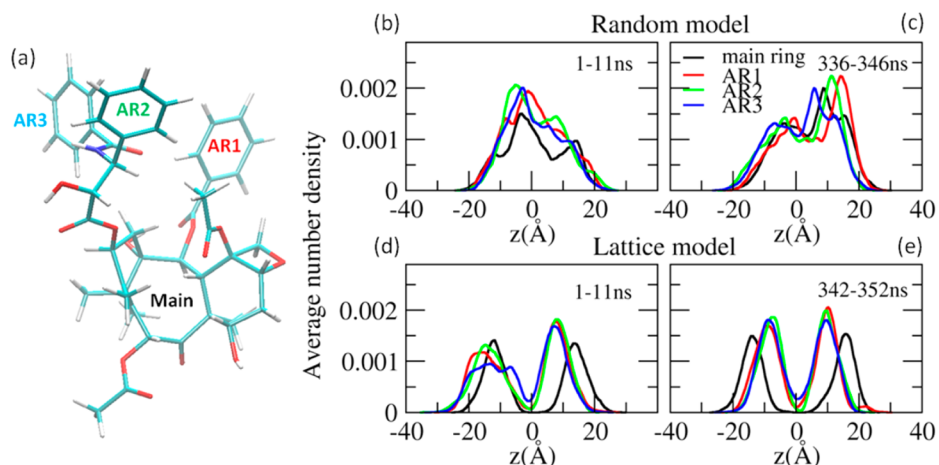


**Figure 6.** Preferred positioning and orientation of each portion of paclitaxel in the membrane. (a) Structure of paclitaxel. The main taxane ring and three phenyl groups, AR1, AR2, and AR3, are in black, red, green, and blue, respectively, which correspond to the colors in the graphs. Average number density of the random model at the beginning 10 ns (b) and the last 10 ns (c) of simulation. Average number density of the lattice model at the beginning of simulation (d) and after simulation (e).

Furthermore, the order parameter of the POPC tails with 12 mol % paclitaxel in the random model decreases compared to that of pure POPC, which indicates an increase of disorder in the tail configurations with the high-concentration drug (Figure 7). This contributes to the stabilization of paclitaxel in the

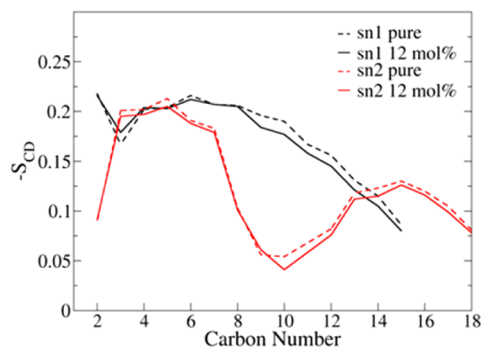


**Figure 7.** Order parameters of the POPC tails in pure POPC (dotted lines) and in POPC with 12 mol % paclitaxel in the random model (solid lines).

membrane containing the drug at the high-concentration limit. Other typical measurements of the membrane properties of pure POPC, including the area per lipid, the thickness, and the electron density profile, are provided in the Supporting Information (Figure S7 and Table S1) and have a good agreement with the experimental data and the previously reported calculations, indicating the convergence of the physicochemical properties of the studied membranes.

The permeability of water into the membrane also increases at the high-concentration limit. Figure 8 compares the water permeability in both the pure and 12 mol % paclitaxel cases. Water molecules penetrate the membrane in the form of transient pores or “water fingers” proximal to the transmembrane clusters of paclitaxel. When a water molecule is

located between the center of P atoms in the top leaflet and that of the bottom leaflet, it is considered to be in the membrane. The number of water molecules in the membrane per POPC molecule increased from  $4.3 \pm 0.1$  water molecules in the pure membrane to  $5.5 \pm 0.1$  water molecules with 12 mol % drug. The depth of water molecules in the membrane also increases. More water molecules are found in proximity of the paclitaxel aggregates. As the drug molecules aggregate at the high-concentration limit, the aggregates span into the core of the membrane and in turn water can access the core of the membrane. Water fingers have been observed in previous simulations of solute–membrane interactions,<sup>61</sup> however, this is the first observation of water mediation by clusters of hydrophobic drugs with simulation.

## CONCLUSION

In this study, we performed all-atom simulations of the hydrophobic anticancer drug paclitaxel in the membrane to investigate its physical interactions in the membrane at the high-concentration limit. The calculated free energy reveals that the distribution and the transportability of the drug in the membrane are affected by the concentration, resulting in a more favorable insertion of the following incoming drug molecules. The free energy minimum shifts toward the hydrophobic core of the membrane, and the central barrier also decreases. The drug molecules rotate and orient along with the membrane in the  $z$  axis so that the hydrophobicity of the drug components matches the local environment of the membrane, but as the aggregates grow, the symmetry is broken. Furthermore, at the high-concentration limit the aggregates enhance the permeability of water within the membrane.

This study is one of the first that demonstrates the concentration-dependent behavior of a hydrophobic drug in a biomembrane utilizing molecular dynamics techniques.<sup>62</sup> For example, Posokhov et al. analyzed the structural properties of a

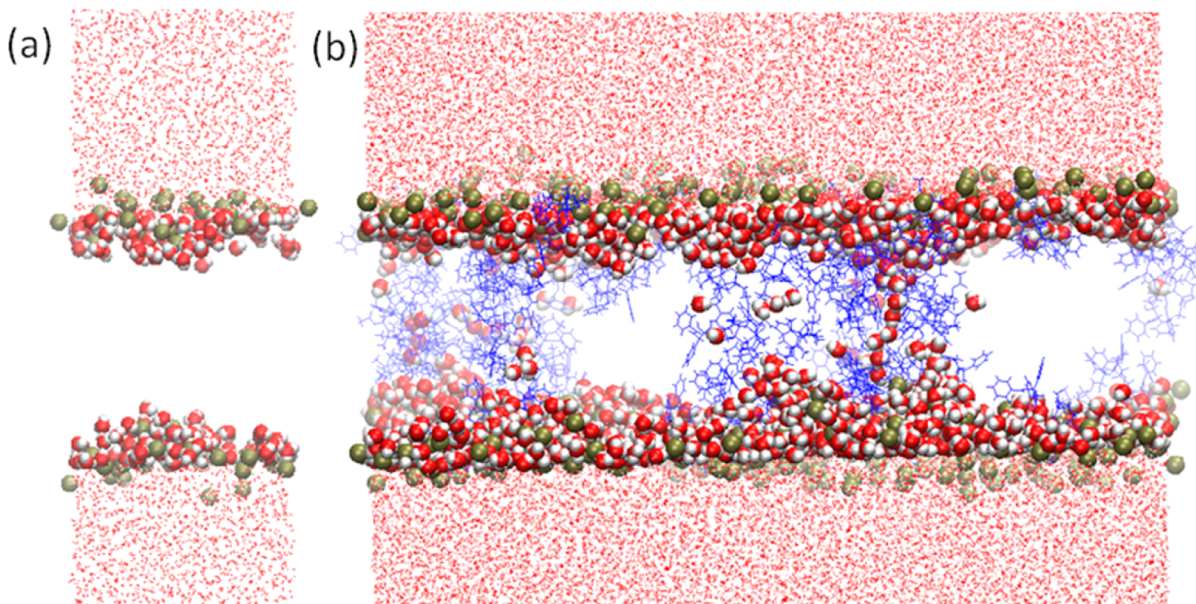


**Figure 8.** Permeability of water in the pure POPC membrane (a) and in POPC with 12 mol % paclitaxel (b). P atoms in the headgroup of POPC are in gold. Water molecules between the center of mass of P atoms in the top leaflet and that of the bottom leaflet are highlighted in red and white VDW space-filled representations. The rest of water and paclitaxel are displayed in red and blue lines, respectively. The rest of the POPC lipids are not shown for clarity.

model POPC membrane with different concentrations of acetone. They observed drastic disordering of membrane packing at accumulations of higher concentrations of the solute,<sup>82</sup> which is consistent with our observation of a decrease in the lipid tail order parameter at higher concentrations of paclitaxel. Although our atomistic simulations of the high concentration of drug in the membrane provide detailed insight into the behavior of the drug in the membrane, they do not give the full picture of the whole membrane-crossing event of the drug due to the limited time scale which atomistic MD simulations can reach. We can perform multiscale simulations,<sup>30,51</sup> including refined coarse-grained models, to further study the whole process and even include important players in drug delivery, such as drug carriers, membrane proteins, and the crowding effect. A better understanding of the interactions between hydrophobic drugs and model membranes at a molecular level will help in designing more efficient drug delivery systems.

## ASSOCIATED CONTENT

### Supporting Information

Figures for the convergence of PMF calculation, decomposition of the interaction energy, clustering over time, orientation of the drug, and diffusion coefficients of paclitaxel in the *z* direction. This material is available free of charge via the Internet at <http://pubs.acs.org>.

## AUTHOR INFORMATION

### Corresponding Author

\*E-mail: sharon.loverde@csi.cuny.edu.

### Notes

The authors declare no competing financial interest.

## ACKNOWLEDGMENTS

This research was supported, in part, by the National Science Foundation (NSF) through TeraGrid resources under Grant TG-CHE130099 and grants of computer time from the City University of New York High Performance Computing Center (NSF Grants CNS-0855217, CNS-0958379, and ACI-1126113). S.M.L. acknowledges startup funding received from the College of Staten Island and City University of New York.

## ABBREVIATIONS

POPC, 1-palmitoyl-2-oleoyl-sn-glycero-3-phosphocholine; ABF, adaptive biasing force; SMD, steered molecular dynamics

## REFERENCES

- (1) Herce, H. D.; Garcia, A. E. Molecular Dynamics Simulations Suggest a Mechanism for Translocation of the Hiv-1 Tat Peptide across Lipid Membranes. *Proc. Natl. Acad. Sci. U.S.A.* **2007**, *104*, 20805–20810.
- (2) Missner, A.; Kuegler, P.; Antonenko, Y. N.; Pohl, P. Passive Transport across Bilayer Lipid Membranes: Overton Continues To Rule. *Proc. Natl. Acad. Sci. U.S.A.* **2008**, *105*, E123–E123.
- (3) Missner, A.; Pohl, P. 110 Years of the Meyer-Overton Rule: Predicting Membrane Permeability of Gases and Other Small Compounds. *ChemPhysChem* **2009**, *10*, 1405–1414.
- (4) Marrink, S.; a. B, H. Simulation of Water Transport through a Lipid Membrane. *J. Phys. Chem.* **1994**, *98*, 4155–4168.
- (5) Diamond, J. M.; Katz, Y. Interpretation of Nonelectrolyte Partition Coefficients between Dimyristoyl Lecithin and Water. *J. Membr. Biol.* **1974**, *17*, 121–154.
- (6) Finkelstein, A.; Cass, A. Effect of Cholesterol on the Water Permeability of Thin Lipid Membranes. *Nature* **1967**, *216*, 717–718.
- (7) Cass, A.; Finkelstein, A. Water Permeability of Thin Lipid Membranes. *J. Gen. Physiol.* **1967**, *50*, 1765–1784.
- (8) Gensure, R. H.; Zeidel, M. L.; Hill, W. G. Lipid Raft Components Cholesterol and Sphingomyelin Increase H<sup>+</sup>/OH<sup>-</sup> Permeability of Phosphatidylcholine Membranes. *Biochem. J.* **2006**, *398*, 485–495.
- (9) Wennberg, C. L.; van der Spoel, D.; Hub, J. S. Large Influence of Cholesterol on Solute Partitioning into Lipid Membranes. *J. Am. Chem. Soc.* **2012**, *134*, 5351–5361.
- (10) Schiff, P. B.; Fant, J.; Horwitz, S. B. Promotion of Micro Tubule Assembly *in Vitro* by Taxol. *Nature (London)* **1979**, *277*, 665–667.
- (11) Jordan, M. A.; Wilson, L. Microtubules as a Target for Anticancer Drugs. *Nat. Rev. Cancer* **2004**, *4*, 253–265.
- (12) Amos, L. A. What Tubulin Drugs Tell Us about Microtubule Structure and Dynamics. *Semin. Cell Dev. Biol.* **2011**, *22*, 916–926.
- (13) Lowe, J.; Li, H.; Downing, K. H.; Nogales, E. Refined Structure of αβ-Tubulin at 3.5 Å Resolution. *J. Mol. Biol.* **2001**, *313*, 1045–1057.
- (14) Mastropaoletto. Crystal and Molecular Structure of Paclitaxel. *Proc. Natl. Acad. Sci. U.S.A.* **1995**, *92*, 6920–6924.
- (15) Balasubramanian, S.; Alderfer, J. L.; Staubinger, R. M. Solvent- and Concentration-Dependent Molecular Interactions of Taxol. *J. Pharm. Sci.* **1994**, *83*, 1470–1476.
- (16) Ashrafuzzaman, M.; Tseng, C. Y.; Duszyk, M.; Tuszyński, J. A. Chemotherapy Drugs Form Ion Pores in Membranes Due to Physical Interactions with Lipids. *Chem. Biol. Drug Des.* **2012**, *80*, 992–1002.
- (17) Koudelka, S.; Turanek, J. Liposomal Paclitaxel Formulations. *J. Controlled Release* **2012**, *163*, 322–334.
- (18) Zhang, Z.; Mei, L.; Feng, S.-S. Paclitaxel Drug Delivery Systems. *Expert Opin. Drug Delivery* **2013**, *10*, 325–340.
- (19) Fahr, A.; van Hoogeveest, P.; May, S.; Bergstrand, N.; Leigh, M. L. S. Transfer of Lipophilic Drugs between Liposomal Membranes and Biological Interfaces: Consequences for Drug Delivery. *Eur. J. Pharm. Sci.* **2005**, *26*, 251–265.
- (20) Gao, Y.; Kuang, Y.; Guo, Z.-F.; Guo, Z.; Krauss, I. J.; Xu, B. Enzyme-Instructed Molecular Self-Assembly Confers Nanofibers and a Supramolecular Hydrogel of Taxol Derivative. *J. Am. Chem. Soc.* **2009**, *131*, 13576–13577.
- (21) Thierry, B.; Kujawa, P.; Tkaczyk, C.; Winnik, F. M.; Bilodeau, L.; Tabrizian, M. Delivery Platform for Hydrophobic Drugs: Prodrug Approach Combined with Self-Assembled Multilayers. *J. Am. Chem. Soc.* **2005**, *127*, 1626–1627.
- (22) Peer, D.; Karp, J. M.; Hong, S.; Farokhzad, O. C.; Margalit, R.; Langer, R. Nanocarriers as an Emerging Platform for Cancer Therapy. *Nat. Nanotechnol.* **2007**, *2*, 751–760.
- (23) Kataoka, K.; Matsumoto, T.; Yokoyama, M.; Okano, T.; Sakurai, Y.; Fukushima, S.; Okamoto, K.; Kwon, G. S. Doxorubicin-Loaded Poly(ethylene glycol)-Poly(β-benzyl-L-aspartate) Copolymer Micelles: Their Pharmaceutical Characteristics and Biological Significance. *J. Controlled Release* **2000**, *64*, 143–153.
- (24) Torchilin, V. P. Recent Advances with Liposomes as Pharmaceutical Carriers. *Nat. Rev. Drug Discovery* **2005**, *4*, 145–160.
- (25) Champion, J. A.; Mitragotri, S. Role of Target Geometry in Phagocytosis. *Proc. Natl. Acad. Sci. U.S.A.* **2006**, *103*, 4930–4934.
- (26) Champion, J. A.; Katre, Y. K.; Mitragotri, S. Making Polymeric Micro- and Nanoparticles of Complex Shapes. *Proc. Natl. Acad. Sci. U.S.A.* **2007**, *104*, 11901–11904.
- (27) Geng, Y.; Dalheimer, P.; Cai, S.; Tsai, R.; Tewari, M.; Minko, T.; Discher, D. E. Shape Effects of Filaments versus Spherical Particles in Flow and Drug Delivery. *Nat. Nanotechnol.* **2007**, *2*, 249–255.
- (28) Gratton, S. E.; Ropp, P. A.; Pohlhaus, P. D.; Luft, J. C.; Madden, V. J.; Napier, M. E.; DeSimone, J. M. The Effect of Particle Design on Cellular Internalization Pathways. *Proc. Natl. Acad. Sci. U.S.A.* **2008**, *105*, 11613–11618.
- (29) Loverde, S. M.; Pantano, D. A.; Christian, D. A.; Mahmud, A.; Klein, M. L.; Discher, D. E. Curvature, Rigidity, and Pattern Formation in Functional Polymer Micelles and Vesicles—From Dynamic Visualization to Molecular Simulation. *Curr. Opin Solid State Mater. Sci.* **2011**, *15*, 277–284.
- (30) Loverde, S. M.; Klein, M. L.; Discher, D. E. Nanoparticle Shape Improves Delivery: Rational Coarse Grain Molecular Dynamics (rCG-

- MD) of Taxol in Worm-like PEG-PCL Micelles. *Adv. Mater.* **2012**, *24*, 3823–3830.
- (31) Kopec, W.; Telenius, J.; Khandelia, H. Molecular Dynamics Simulations of the Interactions of Medicinal Plant Extracts and Drugs with Lipid Bilayer Membranes. *FEBS J.* **2013**, *280*, 2785–2805.
- (32) Loverde, S. M. Molecular Simulation of the Transport of Drugs across Model Membranes. *J. Phys. Chem. Lett.* **2014**, *5*, 1659–1665.
- (33) Ajikumar, P. K.; Xiao, W. H.; Tyo, K. E.; Wang, Y.; Simeon, F.; Leonard, E.; Mucha, O.; Phon, T. H.; Pfeifer, B.; Stephanopoulos, G. Isoprenoid Pathway Optimization for Taxol Precursor Overproduction in *Escherichia coli*. *Science* **2010**, *330*, 70–74.
- (34) Campbell, R. B.; Balasubramanian, S. V.; Straubinger, R. M. Influence of Cationic Lipids on the Stability and Membrane Properties of Paclitaxel-Containing Liposomes. *J. Pharm. Sci.* **2001**, *90*, 1091–1105.
- (35) Huang, H. W. Free Energies of Molecular Bound States in Lipid Bilayers: Lethal Concentrations of Antimicrobial Peptides. *Biophys. J.* **2009**, *96*, 3263–3272.
- (36) Boggara, M. B.; Mihailescu, M.; Krishnamoorti, R. Structural Association of Nonsteroidal Anti-Inflammatory Drugs with Lipid Membranes. *J. Am. Chem. Soc.* **2012**, *134*, 19669–19676.
- (37) Darve, E.; Pohorille, A. Calculating Free Energies Using Average Force. *J. Chem. Phys.* **2001**, *115*, 9169–9183.
- (38) Henin, J.; Fiorin, G.; Chipot, C.; Klein, M. L. Exploring Multidimensional Free Energy Landscapes Using Time-Dependent Biases on Collective Variables. *J. Chem. Theory Comput.* **2010**, *6*, 35–47.
- (39) Brooks, B. R.; Brooks, C. L., III; Mackerell, A. D., Jr.; Nilsson, L.; Petrella, R. J.; Roux, B.; Won, Y.; Archontis, G.; Bartels, C.; Boresch, S.; et al. CHARMM: The Biomolecular Simulation Program. *J. Comput. Chem.* **2009**, *30*, 1545–1614.
- (40) Brooks, B. R.; Bruccoleri, R. E.; Olafson, B. D.; States, D. J.; Swaminathan, S.; Karplus, M. CHARMM: A Program for Macromolecular Energy, Minimization, and Dynamics Calculations. *J. Comput. Chem.* **1983**, *4*, 187–217.
- (41) Klauda, J. B.; Monje, V.; Kim, T.; Im, W. Improving the CHARMM Force Field for Polyunsaturated Fatty Acid Chains. *J. Phys. Chem. B* **2012**, *116*, 9424–9431.
- (42) Neria, E.; Fischer, S.; Karplus, M. Simulation of Activation Free Energies in Molecular Systems. *J. Chem. Phys.* **1996**, *105*, 1902–1921.
- (43) Durell, S. R.; Brooks, B. R.; Ben-Naim, A. Solvent-Induced Forces between Two Hydrophilic Groups. *J. Phys. Chem.* **1994**, *98*, 2198–2202.
- (44) Mitra, A.; Sept, D. Taxol Allosterically Alters the Dynamics of the Tubulin Dimer and Increases the Flexibility of Microtubules. *Biophys. J.* **2008**, *95*, 3252–3258.
- (45) Phillips, J. C.; Braun, R.; Wang, W.; Gumbart, J.; Tajkhorshid, E.; Villa, E.; Chipot, C.; Skeel, R. D.; Kale, L.; Schulten, K. Scalable Molecular Dynamics with NAMD. *J. Comput. Chem.* **2005**, *26*, 1781–1802.
- (46) Martyna, G. J.; Tobias, D. J.; Klein, M. L. Constant Pressure Molecular Dynamics Algorithms. *J. Chem. Phys.* **1994**, *101*, 4177–4189.
- (47) Feller, S. E.; Zhang, Y.; Pastor, R. W.; Brooks, B. R. Constant Pressure Molecular Dynamics Simulation: The Langevin Piston Method. *J. Chem. Phys.* **1995**, *103*, 4613–4621.
- (48) Darden, T.; York, D.; Pedersen, L. Particle Mesh Ewald: An  $N \cdot \text{Log}(N)$  Method for Ewald Sums in Large Systems. *J. Chem. Phys.* **1993**, *98*, 10089–10092.
- (49) Darve, E.; Rodriguez-Gomez, D.; Pohorille, A. Adaptive Biasing Force Method for Scalar and Vector Free Energy Calculations. *J. Chem. Phys.* **2008**, *128*, 144120.
- (50) Wenk, M. R.; Fahr, A.; Reszka, R.; Seelig, J. Paclitaxel Partitioning into Lipid Bilayers. *J. Pharm. Sci.* **1996**, *85*, 228–231.
- (51) Orsi, M.; Essex, J. W. Permeability of Drugs and Hormones through a Lipid Bilayer: Insights from Dual-Resolution Molecular Dynamics. *Soft Matter* **2010**, *6*, 3797–3808.
- (52) Ellis, R. J. Macromolecular Crowding: An Important but Neglected Aspect of the Intracellular Environment. *Curr. Opin Struct. Biol.* **2001**, *11*, 114–119.
- (53) Scheve, C. S.; Gonzales, P. A.; Momin, N.; Stachowiak, J. C. Steric Pressure between Membrane-Bound Proteins Opposes Lipid Phase Separation. *J. Am. Chem. Soc.* **2013**, *135*, 1185–1188.
- (54) Niemela, P. S.; Miettinen, M. S.; Monticelli, L.; Hammaren, H.; Bjelkmar, P.; Murtola, T.; Lindahl, E.; Vattulainen, I. Membrane Proteins Diffuse as Dynamic Complexes with Lipids. *J. Am. Chem. Soc.* **2010**, *132*, 7574–7575.
- (55) Stachowiak, J. C.; Schmid, E. M.; Ryan, C. J.; Ann, H. S.; Sasaki, D. Y.; Sherman, M. B.; Geissler, P. L.; Fletcher, D. A.; Hayden, C. C. Membrane Bending by Protein-Protein Crowding. *Nat. Cell Biol.* **2012**, *14*, 944–949.
- (56) Cramariuc, O.; Rog, T.; Javanainen, M.; Monticelli, L.; Polishchuk, A. V.; Vattulainen, I. Mechanism for Translocation of Fluoroquinolones across Lipid Membranes. *Biochim. Biophys. Acta, Biomembr.* **2012**, *1818*, 2563–2571.
- (57) Kopec, W.; Khandelia, H. Reinforcing the Membrane-Mediated Mechanism of Action of the Anti-Tuberculosis Candidate Drug Thioridazine with Molecular Simulations. *J. Comput.-Aided Mol. Des.* **2014**, *28*, 123–134.
- (58) Iannuzzi, M.; Laio, A.; Parrinello, M. Efficient Exploration of Reactive Potential Energy Surfaces Using Car-Parrinello Molecular Dynamics. *Phys. Rev. Lett.* **2003**, *90*, 238302.
- (59) Stokes, G. G. *Mathematical and Physical Papers*; Cambridge University Press: Cambridge, U.K., 1880.
- (60) Einstein, A. *Brownian Movement*; Dover: New York, 1956.
- (61) Ulander, J.; Haymet, A. D. J. Permeation across Hydrated DPPC Lipid Bilayers: Simulation of the Titratable Amphiphilic Drug Valproic Acid. *Biophys. J.* **2003**, *85*, 3475–3484.
- (62) Posokhov, Y. O.; Kyrychenko, A. Effect of Acetone Accumulation on Structure and Dynamics of Lipid Membranes Studied by Molecular Dynamics Simulations. *Comput. Biol. Chem.* **2013**, *46*, 23–31.